Raman activity of the longitudinal optical phonons of the LiNbO 3 crystal: Experimental determination and quantum mechanical simulation

Bernardo A. Nogueira, Michel Rérat, Rui Fausto, Chiara Castiglioni, Roberto Dovesi

Received: 8 June 2022 | Revised: 11 July 2022 | Accepted: 14 July 2022

DOI: 10.1002/jrs.6426

RESEARCH ARTICLE

Journal of RAMAN SPECTROSCOPY WILEY

Raman activity of the longitudinal optical phonons of the $LiNbO_3$ crystal: Experimental determination and quantum mechanical simulation

Bernardo A. Nogueira[1] | **Michel Rérat**[2] | **Rui Fausto**[1] | **Chiara Castiglioni**[3] | **Roberto Dovesi**[4]

[1]CQC-IMS, Department of Chemistry, University of Coimbra, Coimbra, Portugal

[2]Université de Pau et des Pays de l' Adour, CNRS, IPREM, E2S UPPA, Pau, France

[3]Dipartimento di Chimica Materiali e Ingegneria Chimica Giulio Natta, Politecnico di Milano, Milan, Italy

[4]Dipartimento di Chimica, Università di Torino and NIS (Nanostructured Interfaces and Surfaces) Centre, Torino, Italy

Correspondence
Chiara Castiglioni, Dipartimento di Chimica Materiali e Ingegneria Chimica Giulio Natta, Politecnico di Milano, piazza Leonardo da Vinci, 32, Milan 20133, Italy.
Email: chiara.castiglioni@polimi.it

Funding information
Fundação para a Ciência e a Tecnologia, Grant/Award Numbers: UIDB/00313/2020, UIDP/00313/2020, SFRH/BD/129852/2017

Abstract

In this study, the $Y(XX)\overline{Y}$ and the two equivalent $Z(XX)\overline{Z}/Z(YY)\overline{Z}$ polarized Raman spectra of a $LiNbO_3$ single crystal have been recorded and used as a benchmark test for the density functional theory (DFT) calculation of the longitudinal modes and of their Raman activity. The theoretical approach, based on periodic boundary conditions and a linear combination of atomic orbitals (LCAO), provides excellent predictions of phonon wavenumbers and relative bands intensities for both A_1 and E Longitudinal Optical (LO) modes and complements a previous paper limited to the study of Transverse Optical (TO) modes. Overall, the present investigation demonstrates that the LCAO approach, as implemented in the CRYSTAL software, gives results of similar accuracy for the TO and the LO phonons features. By means of a band deconvolution scheme applied to the experimental spectra, we present, for the first time, a quantitative comparison between experimental and theoretically predicted polarized Raman band intensities of $LiNbO_3$ LO modes. This analysis highlights the role of the suitable determination of the static and high-frequency dielectric matrices that are needed for the prediction of the TO/LO frequency split but also the first nonlinear electric susceptibility tensor for an accurate description of the Raman intensity pattern.

KEYWORDS

CRYSTAL software, DFT simulations, LO modes, polarized Raman, Raman activity

1 | INTRODUCTION

Raman and IR spectroscopies provide tools for the structural characterization of crystals through the experimental determination of their phonon properties, which allow distinguishing among different crystalline phases,[1–4] and are sensitive to the presence of chemical and structural defects.[5,6] Moreover, polarized vibrational spectra can highlight the macroscopic orientation of the crystalline system when the point symmetry is sufficiently high.[7–11] Quantum Mechanical simulation is nowadays a ripe instrument for the generation of

accurate IR and Raman spectra that can be used as a complement, in some instances, or as an alternative, in other instances, to the experiment.[12–15] On the other hand, the availability of the spectra of high purity single crystals with known structure, suitably oriented in the laboratory framework, can provide a rich set of spectroscopic data, which allow to accurately check the theoretical methods developed for the first principles prediction of crystal structures and their physical properties.

In a recent study,[16] the density functional theory (DFT) has been used with linear combination of atomic orbitals (LAO) to calculate the Raman spectrum of the ferroelectric *R3c* $LiNbO_3$ crystal. The relative Raman intensities of the transverse optical (TO) phonons of A_1 and E symmetry, calculated with the CRYSTAL software,[17] resulted in a remarkable improvement over previously reported calculations.[18,19]

In this paper, we extend the comparison to the longitudinal optical (LO) modes of the Raman spectrum. The LO modes not only increase the set of data (from 13 to 26 wavenumbers and relative Raman intensities) on which the comparison with experiment is performed but also represent a challenge for further tools implemented in the computer code and for experimental equipment. Furthermore, additional checks are possible comparing the TO and LO components of the spectra; at the same time, this comparison provides additional understanding on the electronic and dynamical nature of the compound under investigation.

The experimental Raman spectra of a single oriented crystal of $LiNbO_3$ have been obtained in backscattering mode, according to different polarization setup. This allows extracting information about the elements of the Raman polarizability tensor, which determine the Raman activity of LO modes in the different experiments. In particular, the $Y(XX)\overline{Y}$ experimental configuration selects TO A_1 phonons transitions together with LO E transitions, while the two equivalent $Z(XX)\overline{Z}/Z(YY)\overline{Z}$ configurations allow investigating LO A_1 phonons and TO E phonons.

These experimental spectra have been reproduced from computed polarizability tensor elements associated to the active TO and LO phonons, thus providing a further test about the quality of LO versus TO modes description.

The direct comparison with the experimental data provides the assessment of the predictive capability of the adopted theoretical method, while a discussion of the results obtained in Hermet et al.[20] allows a comparison between two different theoretical approaches.

As in the case of TO modes, already discussed in Nogueira et al.,[16] we obtained a very good agreement between predicted and experimental vibrational wavenumbers of the LO phonons. Our bands' assignment of $LiNbO_3$ supports in general the vibrational assignments proposed by Hermet et al.[20] On the contrary, some non-negligible differences from Hermet et al.[20] appear in the description of TO/LO modes shifts and overlaps.

The obtained results confirm the reliability of the theoretical approach here adopted for a thorough investigation of the structure and phonons properties of the $LiNbO_3$ crystal; together with the analysis reported in our previous study,[16] the procedure here illustrated can be considered a benchmark test for simulations of the phonons of crystalline materials.

2 | MATERIAL AND METHODS

2.1 | Computational details

The calculation of the TO Raman spectra[16] has been extended to LO in the current study.

The CRYSTAL code,[17,21] the B3LYP functional[22] and the pob-TZVP basis set[23–25] have been used. The geometry has been optimized (*R3c* space group), and the TO Raman spectra have been computed, at first. The high-frequency dielectric tensor has also been computed, as an ingredient for the prediction of the LO spectrum. The derivatives of the polarizability with respect to the atomic displacements have been calculated at the coupled-perturbed Hartree-Fock (CPHF) or Kohn-Sham (CPKS) level.[26–28]

The starting geometry was the one experimentally determined by Abrahams et al.[29]

Vibrational wavenumbers were computed by diagonalizing the dynamical matrix at the Γ point of the first Brillouin zone (BZ) and the Cartesian force constants (i.e., the elements of the Hessian of the potential energy, expressed in mass-weighted atomic Cartesian coordinates) were computed by numerical derivation of the analytical gradients.

In the case of ionic systems for which Born charges (variations of the dipole moment with respect to atomic displacements) are not null, a corrective term to the dynamical matrix that includes the high-frequency dielectric constant must be added,[30] which leads to a splitting between the TO and LO mode wavenumbers.

The Raman activity of the k normal mode, A_{ij}^k, corresponding to incident and scattered beams with i and j polarization direction, respectively, is computed as $A_{ij}^k = \left(\alpha_{ij}^k\right)^2$, where α_{ij}^k is the i,j component of the Raman tensor associated to mode k (derivative of the polarizability with respect to the TO/LO modes). In the limit of

static exciting field ($\lambda_{exc} \to \infty$), Raman Intensities I_{ij}^k can be then computed as $I_{ij}^k = \frac{A_{ij}^k}{\omega_k}$, where ω_k is the vibrational frequency of the normal mode k.

In the case of LO modes, the Raman activity expression above must be corrected by a term depending on $\chi^{(2)}$, the first non-linear electric susceptibility or derivative of the high-frequency dielectric matrix ($\boldsymbol{\varepsilon}$) and Born charges ($\boldsymbol{Z}^*$), due to polarization effects.[31] Indeed, for non-centrosymmetric crystals (for which $\chi^{(2)} \neq \mathbf{0}$), the Raman polarizability tensors, namely, the third derivative of the unit cell energy with respect to once the atomic displacements and twice the electric field, becomes

$$\alpha_{ij}^k \to \alpha_{ij}^k - 2\sum_{i'} Z_{i'}^{*k} \sum_{l} \varepsilon_{i'l}^{-1} \chi_{ijl}^{(2)}. \quad (1)$$

For sake of brevity, we hereafter refer to the second term on the right hand side of Equation (1) as '$\chi^{(2)}$ correction'.

The correspondence between the different components of the calculated polarized Raman spectra and the experimental spectra obtained using the back-scattering mode in a Horiba LabRam HR Evolution Raman spectrometer was established as described below.

2.2 | Experimental spectra collection

The LiNbO3 crystal samples (Y-cut and Z-cut faces; 10 mm × 10 mm × 0.5 mm) were bought from PI-KEM Ltd. Y-cut and Z-cut mean that the crystal face cut is perpendicular to the y and z directions, respectively, of the piezoelectric crystal, being the z axis the polar axis, namely, the direction of the crystal dipole.

Single crystal Raman spectra were obtained in the Raman shift wavenumber range 50–1,000 cm^{-1}, with accuracy better than 0.5 cm^{-1}, using a Raman microsystem Horiba LabRam HR Evolution. The excitation was provided by a solid-state laser $\lambda = 532$ nm (horizontally polarized; laser power ~50 mW). In order to collect the polarized spectra, there were used one half-wave polarization rotator (Horiba-Jobin-Yvon) to rotate the polarization of the incident light and a CorePol P-500-1000 polarizer (Horiba-Jobin-Yvon) to tune the component of the excitation light to collect. The collection time values used were between 2 and 20 s, with 100 accumulations being averaged to produce the final spectra. A 50X objective lens was used, being the laser spot diameter of 1 μm at the sample. The calibration was performed using the characteristic Si wafer band (520.5 cm^{-1}). The experimental setup corresponding to $Y(XX)\overline{Y}$ configuration (TO A_1 + LO E transitions) and $Z(XX)\overline{Z}/Z(YY)\overline{Z}$ (LO A_1 + TO E transitions), corresponding to the spectra presented and discussed in this paper, is illustrated in Figure 1.

3 | LO PHONONS TRANSITIONS IN POLARIZED RAMAN SPECTRA OF $LINBO_3$ CRYSTAL

The 27 $\Gamma = 0$ phonons of the room temperature stable phase ($R3c$) of $LiNbO_3$ can be grouped according to their irreducible representations as 4 A_1, 5 A_2 and 9 E (doubly degenerate), where the A_1 (polarized along z) and the E (polarized in the xy plane) modes are IR and Raman active, whereas the A_2 modes are silent.[20,32] In a Cartesian system where the z axis is aligned along the polar direction of $LiNbO_3$ and x is aligned along the crystallographic axis $\boldsymbol{a}$, the Raman polarizability tensor of the E and A_1 modes show the following structure[33]:

$$E(x) = \begin{pmatrix} c & 0 & d \\ 0 & -c & 0 \\ d & 0 & 0 \end{pmatrix}, E(y) = \begin{pmatrix} 0 & -c & 0 \\ -c & 0 & d \\ 0 & d & 0 \end{pmatrix}, A_1(z) = \begin{pmatrix} a & 0 & 0 \\ 0 & a & 0 \\ 0 & 0 & b \end{pmatrix}.$$

For each Raman active mode, a pair of Raman transitions are observed at different wavenumbers, namely, longitudinal optical (LO) and transverse optical (TO) phonons. The phenomenon has been described several years ago,[34,35] for IR active phonons of polar crystals, as are the ferroelectric ionic crystals.

According to the experimental setup described in Section 2, the intensities of the polarized Raman spectra here analysed depend on the elements

$$c = \alpha_{xx}^k = \frac{\partial \alpha_{xx}}{\partial Q_k^E} = -\alpha_{yy}^k = -\frac{\partial \alpha_{yy}}{\partial Q_k^E}$$

of the E tensors and on the elements

$$a = \alpha_{xx}^k = \frac{\partial \alpha_{xx}}{\partial Q_k^{A1}} = \alpha_{yy}^k = \frac{\partial \alpha_{yy}}{\partial Q_k^{A1.}}$$

of the A_1 tensor.

The b and d elements appearing in the E and A_1 Raman tensors do not contribute to the Raman transitions observed in the polarized spectra discussed in this paper.

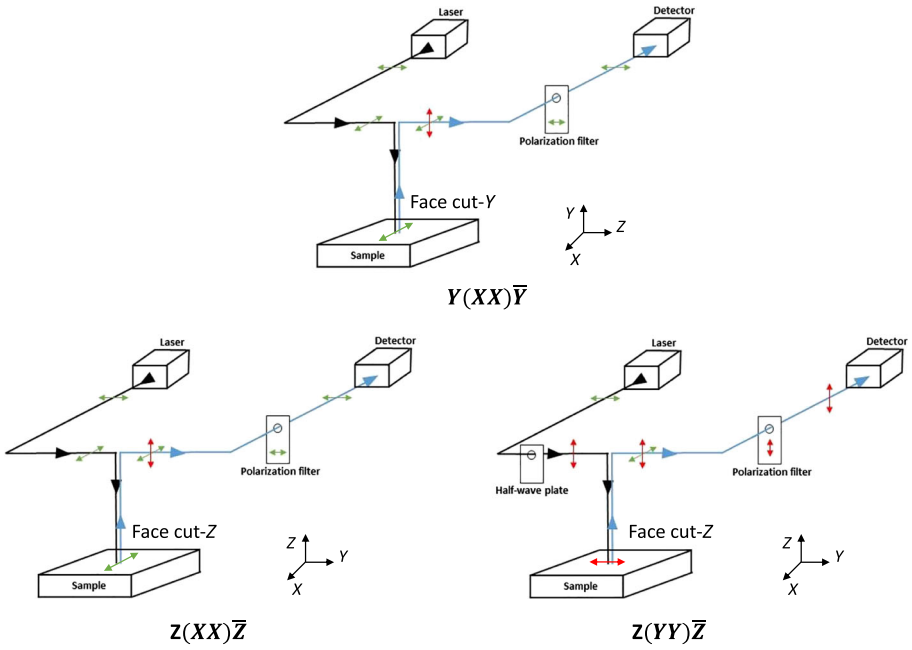

FIGURE 1 Schematic representation of the geometric configurations determining the polarization of the laser beam relatively to the sample in the used instrument (Horiba LabRam HR evolution). The black and blue traces correspond to the incident and scattered beams, respectively. The double arrows represent the direction of the polarization of the beam, classified as horizontal (H) and vertical (V) in the reference frame of the laboratory. The depicted Cartesian vectors, X, Y and Z, refer to the crystal sample reference frame and vary for the different crystal cuts. The shown examples correspond to the two different configurations adopted for recording the spectra here analysed. [Colour figure can be viewed at wileyonlinelibrary.com]

3.1 | Vibrational wavenumbers and Raman spectrum assignment

In Table 1, we summarize wavenumbers and vibrational assignment of the TO e LO phonons of $LiNbO_3$, as obtained according to our calculations. Experimental peak wavenumbers of our recorded spectra are compared with our theoretical predictions. In addition, Table 1 shows the experimental LO phonon wavenumbers reported in a recent review,[36] and the theoretical determinations from Hermet et al.[20] Even if there is a wide literature concerning experimental and theoretical studies of the vibrational spectra of $LiNbO_3$,[20,32,34,36–42] we will limit here the comparison with these two papers, which in our opinion are the most complete and accurate.

In Table 1 (a), we labelled TO modes from the lowest to the highest wavenumber, separately for the E (from 1E to 9E) and A_1 ($1A_1$ to $4A_1$) species. LO modes (Table 1, b) are identified in a similar way, by progressive numbering, while increasing the wavenumber. The first column of Table 1 (b) illustrates (numbers in parentheses) the correlation between LO and TO phonons according to the overlap between mode eigenvectors (see Table S1). In some cases, more than one TO phonon shows a large overlap with a LO mode, and then, more than one TO phonon is associated to it in Table 1 (b). In the second column of Table 1 (b), we list (values in parentheses) the shift ($\Delta\nu$) of the Raman wavenumber of LO modes, with respect to the wavenumber of the correlated TO modes. In this way, we can identify $4A_1$ and 9E as the LO modes most affected by the correction of the dynamical matrix and, to a lesser extent, $3A_1$ and 7E modes. Among these modes, only 9E shows a large overlap with one only TO mode (8E), while the other three modes correlate (large overlap) with more than one TO mode.

Considering the TO/LO pairs showing the largest overlap, we observe a very large frequency split for the pairs ($1A_1$(TO), $3A_1$(LO)); (8E(TO), 9E(LO)); ($4A_1$(TO), $4A_1$(LO)). The computed IR intensities of the TO modes (Table S2) explain these large shifts.

Among the TO phonons of E species, the mode 8E shows a remarkably high intensity, more than twice larger than the strong 1E, 3E, 4E IR transitions; among the A_1 TO phonons, IR intensities of $1A_1$ and $4A_1$ are the largest ones. LO modes correlated to TO modes carrying a large dipole moment fluctuation (8E, $1A_1$ and $4A_1$) are expected to have the largest TO/LO frequency splitting, and indeed this is what has been observed.

The assignment of the experimental peak wavenumbers of TO phonons has been widely discussed in Nogueira et al.[16] Table 2 shows a good correspondence

TABLE 1 Comparison between the predicted Raman shifts (cm^{-1}) for TO and LO modes of the $LiNbO_3$ crystal

a. TO MODES				b. LO MODES				
Mode	**Theory**	**Theory (Hermet et al.[20])**	**Exp**	**Mode**	**Theory**	**Theory (Hermet et al.[20])**	**Exp**	**Exp (Fontana & Bourson[36])**
irrep	**ν (cm^{-1})**	**ν (cm^{-1})**	**ν (cm^{-1})**	**irrep (#TO)**	**ν (cm^{-1}) ($\Delta\nu_{LO-TO}$)**	**ν (cm^{-1})**	**ν (cm^{-1})**	**ν (cm^{-1}) (#mode)**
1E	159	155	152	1E (1)	195 (+36)	197	191	194 (2)
2E	240	218	237	2E (2)	242 (+2)	224	236	238 (3)
$1A_1$	256	243	252	$1A_1$ (**2**;1)	276 (−3; 2)	287	273	
3E	266	264	261	3E(**3**;**4**)	296 (+30; −24)	298	295	295 (4)
$2A_1$	279	288	274	$2A_1$ (3)	342 (0)	348	333	332 (2)
4E	320	330	320	$3A_1$(**1**;4)	434 (+178;−201)	413	426	419 (3)
$3A_1$	342	355	331	4E (4;**5**)	344 (+44;−8)	349	332	?
5E	352	372	359	5E (6)	368 (−1)	384	369	366 (5)
6E	369	384	369	6E (7)	431 (−14)	423	424	425 (6)
7E	445	428	432	7E (**7**;**8**)	466 (+21;−107)	452	465	456 (7)
8E	588	585	579	8 E (9)	663 (−3)	675	683	625 (8)
$4A_1$	635	617	632	$4A_1$ (**4**;1)	883 (+248; +627)	855	872	871 (4)
9 E	666	677	670	9E (8)	892 (+304)	863	880	880 (9)

Note: Calculated wavenumbers according to our work and Hermet et al.[20] TO and LO phonons are numbered from the lowest to the highest wavenumber, separately for A_1 and E symmetry species. The first column of (b) indicates (numbers in parentheses) the correlation between LO and TO phonons according to the overlap (LO phonon eigenvectors showing overlap values ≥ 0.4 with the TO eigenvectors are considered). Boldface characters highlight the TO mode showing the largest overlap with the associated LO mode, in cases where more than one TO mode satisfies the above condition. LO/TO wavenumber split is reported ((b), column II, values in parenthesis). Experimental wavenumbers of LO modes determined in this work and in Fontana and Bourson[36] are reported in (b), columns IV, V; in (b), column V, the assignment according to Fontana and Bourson[36] is indicated in parentheses.

TABLE 2 Comparison between our predicted and experimental wavenumbers (cm^{-1}) of the Raman active phonons of $LiNbO_3$

TO MODES					LO MODES				
Mode	**ν_{theo}**	**ν_{exp}**	**$\Delta\nu$**	**Err%**	**Mode**	**ν_{theo}**	**ν_{exp}**	**$\Delta\nu$**	**Err%**
1E	159	152	7	4.605	1E	195	191	4	2.094
2E	240	237	3	1.266	2E	242	236	6	2.542
$1A_1$	256	252	4	1.587	$1A_1$	276	273	3	1.099
3E	266	261	5	1.916	3E	296	295	1	0.339
$2A_1$	279	274	5	1.825	$2A_1$	342	333	9	2.703
4E	320	320	0	0.000	4E	344	332	**12**	3.614
$3A_1$	342	331	**11**	3.323	5E	368	369	-1	−0.271
5E	352	359	−7	−1.950	6E	431	424	7	1.651
6E	369	369	0	0.000	$3A_1$	434	426	8	1.878
7E	445	432	**13**	3.009	7E	466	465	1	0.215
8E	588	579	9	1.554	8E	663	683	**−20**	−2.928
$4A_1$	635	632	3	0.475	$4A_1$	883	872	**11**	1.261
9E	666	670	−4	−0.597	9E	892	880	**12**	1.364

Note: Boldface characters indicate differences ($\Delta\nu$) exceeding 10 cm^{-1}.

between our predicted wavenumbers and the Raman shifts that we determined experimentally. The quality of the agreement is similar to (in some cases) or better than (in other cases) the one obtained in Hermet et al.[20]

In Table 2, the differences ($\Delta\nu$) between the theoretical and experimental wavenumbers are reported. Among the 13 TO computed values, only in two cases $\Delta\nu$ has a value larger than 10 cm^{-1} (11 and 13 cm^{-1}). For the LO

modes, there are four values exceeding 10 cm^{-1} (11, 12, 12 and -20 cm^{-1}). By far, the largest difference ($\Delta\nu = -20$ cm^{-1}) is for the 8E mode, whose experimental determination is however questionable, due to its very low Raman intensity (see below). The Mean Absolute Error (MAE) on the full set of 26 modes is as small as 6.4 cm^{-1}.

It should be noticed that in 22 out of 26 cases the simulated values are blue shifted with respect to experiment. A more extensive and complete basis set might probably red shift all wavenumbers and reduce the MAE.

For the five hardest modes with wavenumber between 600 and 700 cm^{-1}, including the A_1-mode of highest Raman intensity, we carried out anharmonic calculations using the vibrational self-consistent-field (VSCF) and configuration interaction (VCI) methods implemented in an in-progress version of the CRYSTAL code.[43–45] The wavenumbers redshift by about 1% (e.g., 635 cm^{-1} → 630 cm^{-1}) for the A_1-mode, and the Raman intensity increases by about 4% (1,000 → 1,037, arbitrary units). For the degenerate less intense E-modes, the anharmonic correction is negligible (588.4 → 588.2 cm^{-1} and 666 → 664 cm^{-1} for the wavenumbers and 305 → 304 and 13.7 → 13.8 a.u. for the intensities).

According to our results, we agree with the assignment by Hermet et al.[20] of the 4E (LO) (predicted at 349 cm^{-1}) to the very weak mode at 332 cm^{-1} (our computed LO wavenumber is at 344 cm^{-1}). In the list of the experimental LO wavenumbers reported by Fontana and Bourson,[36] no experimental determinations close to our prediction for 4E can be found, while in the present work, the 4E (LO) peak has been identified following the suggestion from calculations, due to its very low intensity. In the last column of Table 1, we report the experimental LO modes from Fontana and Bourson,[36] listed according to our assignment, with the indication of the original assignment in parentheses. According to the new assignment, the experimental peak at 186 cm^{-1} assigned to 1E (LO) in Fontana and Bourson[36] must be removed from the list of the fundamental vibrational transitions of $LiNbO_3$.

The correspondence between LO and TO modes, based on the overlap matrices reported in Table S2, shows some discrepancies in the description of the LO phonons eigenvectors compared to the overlap matrices reported in Hermet et al.[20] The major differences regard the description of 4E (LO) and 7E (LO) and, to a lesser extent, 3E (LO). Unfortunately, the two theoretical approaches give very close wavenumbers for these phonons, and their Raman activities are very low, so it is impossible to compare the quality of the two calculations based on their predictive capability of the Raman features associated to these modes.

3.2 | Prediction of polarized Raman intensities and spectra simulation

In this section, we present a detailed comparison between experimental and calculated polarized Raman spectra considering two experimental setups in the backscattering configuration, which allow to collect information about LO and TO modes of the two Raman active symmetry species.

In Table 3, theoretical band intensities corresponding to the $Y(XX)\overline{Y}$ experimental configuration are obtained from the α_{xx} component of the Raman tensor of the E (LO) and A_1 (TO) modes (see equations in Section 2). Their experimental counterparts are obtained from the recorded spectrum, as the area of the individual bands obtained according to a curve deconvolution procedure. The computed and experimental Raman intensities for the two equivalent $Z(XX)\overline{Z}/Z(YY)\overline{Z}$ experimental configurations are reported in Table 4.

The use of a deconvolution procedure is mandatory when the experimental spectral pattern consists in several partially overlapped bands. This is the case of the experimental $Y(XX)\overline{Y}$ spectrum (Figure 2) in the region below 350 cm^{-1} and of the experimental $Z(XX)\overline{Z}/Z(YY)\overline{Z}$ spectrum (Figure 3), in the region between 250 and 500 cm^{-1}.

The bands of the experimental spectra were deconvoluted using the *peak resolve* option available in the Omnic software.[46] The experimental spectra obtained in the two equivalent $Z(XX)\overline{Z}/Z(YY)\overline{Z}$ setups are practically superimposable, so we selected the $Z(XX)\overline{Z}$ spectrum for the analysis.

It is worth noticing that the experimental peak wavenumbers of the individual Raman transitions we have obtained by means of the deconvolution procedure are very close to the ones we previously identified focusing at the bands maxima of the raw spectra (see Tables S3 and S4).

Table 3 shows that the E Raman transitions have a very low activity. Bands associated to TO A_1 phonons transitions dominate the Raman spectrum, showing a very strong $4A_1$ band, which we take as a reference for the determination of the relative Raman intensities, for both the theoretical and the experimental spectra. The other three TO A_1 phonons transitions show intensities about 10 times weaker than the $4A_1$ band. Among the seven LO E transitions, four of them have intensity values of the order of 10^{-2} (relative to 4 A_1 band), and the strongest one is the 6E LO transition, whose intensity amounts to only 4% of the reference line intensity.

Despite these issues, the data reported in Table 3 and the spectra of Figure 2 show that theory and experiments are very consistent. The calculated relative intensities are

TABLE 3 Comparison between computed and experimental (integrals from curve fitting) Raman bands intensities corresponding to the polarized spectrum in the $Y(XX)\overline{Y}$ experimental configuration

Mode	Calculated (experimental) wavenumber (cm^{-1})	Relative Intensity					
		Calculated (a.u.)		Experimental (a.u)		% Err	
1E (LO)	195 (191)	0.003		0.003		0	
2E (LO)	242 (236)	0.009		0.011		−14.4	
$1A_1$ (TO)	256 (252)	0.147	0.302	0.161	*0.322*	−8.7	−6.2
$2A_1$ (TO)	279 (274)	0.125		0.128		−2.2	
3E (LO)	296 (295)	0.021		0.023		−10.3	
$3A_1$ (TO)	342 (331)	0.063	0.064	0.066	*0.068*	−4.3	−5.8
4E (LO)	344 (332)	0.001		0.002		−100	
5E (LO)	368 (369)	0.010		0.017		−41.1	
6E (LO)	431 (424)	0.041		0.048		−14.8	
7 E (LO)	466 (465)	0.000		0.000		0	
$4A_1$ (TO)	**635 (632)**	**1**		**1**		-	
8E (LO)	663 (683)	0.003		0.072		−95.9	
9E (LO)	892 (880)	0.018		0.019		−4.6	

Note: Calculated intensities are obtained from the α_{xx} component of the Raman tensor of the E (LO) and A_1 (TO) modes, which are active in this experimental configuration. The band corresponding to the $4A_1$ (TO) mode was chosen as reference (presented in bold). Intensities in relative arbitrary units (a. u.). Values in italic correspond to sums of bands whose individual experimental intensities result from band deconvolution. For each mode, the percentage error (% Err) with respect to the experimental data was calculated as % Err = ((Relative intensity calculated – Relative intensity experimental)/Relative intensity experimental) × 100.

TABLE 4 Comparison between computed and experimental (integrals from curve fitting) Raman bands intensities corresponding to the polarized spectrum in the $Z(XX)\overline{Z}$ experimental configuration

Mode	Calculated (experimental) wavenumber (cm^{-1})	Relative Raman Intensity					
		Calculated		Experimental		% Err	
1E (TO)	159 (152)	0.126		0.145		−13.2	
2E (TO)	240 (237)	0.075		0.049		52.7	
3E (TO)	266 (261)	0.050	0.160	0.051	*0.166*	−2.3	−3.6
$1A_1$ (LO)	276 (273)	0.110		0.115		−4.0	
4E (TO)	320 (320)	0.039	0.212	0.041	*0.195*	3.2	8.7
$2A_1$ (LO)	342 (333)	0.173		0.154		12.3	
5E (TO)	352 (359)	0.016	0.094	0.021	*0.071*	−22.7	32.4
6E (TO)	369 (369)	0.078		0.050		55.5	
$3A_1$ (LO)	434 (426)	0.360	0.520	0.347	*0.509*	3.8	2.2
7E (TO)	445 (432)	0.160		0.162		−1.2	
8E (TO)	588 (579)	0.164		0.202		−18.8	
9E (TO)	666 (670)	0.048		0.054		−11.3	
$4A_1$ (LO)	**883 (872)**	**1**		**1**			

Note: Calculated intensities are obtained from the α_{xx}/α_{yy} component of the Raman tensor of the E (TO) and A_1 (LO) modes, which are active in the two (equivalent) $Z(XX)\overline{Z}$ / $Z(YY)\overline{Z}$ experimental configuration. The band corresponding to the $4A_1$ (LO) mode was chosen as reference (presented in bold). Intensities in relative arbitrary units (a. u.). Values in italic correspond to sums for bands whose individual intensities result from band deconvolution. For each mode, the percentage error (% Err) with respect to the experimental data was calculated as % Err = ((Relative intensity calculated – Relative intensity experimental)/Relative intensity experimental) × 100.

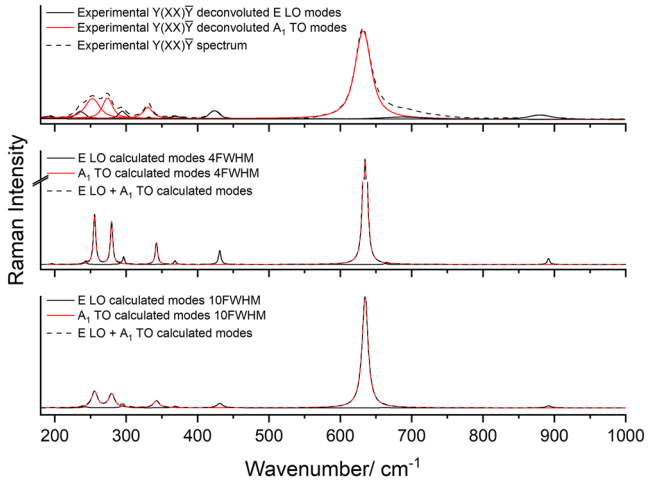

FIGURE 2 Experimental $Y(XX)\overline{Y}$ spectrum of $LiNbO_3$ crystal, and the respective individual deconvoluted bands (*top*) and the calculated spectrum (E LO modes + A_1 TO modes) based on the α_{xx} component of the Raman tensors. Each band is described by a Loretzian function with 4 FWHM (*middle*) and 10 FWHM (*bottom*). [Colour figure can be viewed at wileyonlinelibrary.com]

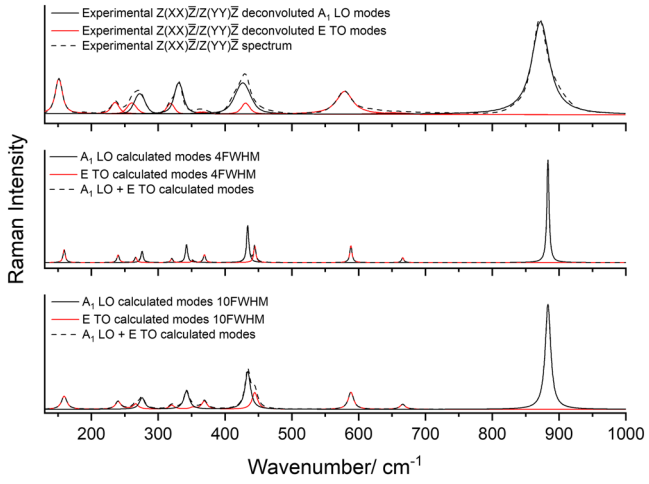

FIGURE 3 Experimental $Z(XX)\overline{Z}$ spectrum of $LiNbO_3$ crystal, and the respective individual deconvoluted bands (*top*) and the calculated spectrum (E TO modes + A_1 LO modes) based on the α_{xx}/α_{yy} component of the Raman tensors. Each band is described by a Lorentzian function with 4 FWHM (middle) and 10 FWHM (*bottom*). [Colour figure can be viewed at wileyonlinelibrary.com]

slightly underestimated with respect to the experimental ones. While considering the two integrated spectral regions, comprehending the Raman transitions between 200 and 300 cm^{-1} and between 300 and 350 cm^{-1}, respectively (see Table 3), in most of the cases, the percentage error of the computed results is about 10%. The results are unsatisfactory for the very weak band corresponding to the 5E LO phonon transition (Err% = 41) and for the practically silent 8E LO mode (Err% = 96): In these cases, the large discrepancy between theory and experiment can be attributed to the large uncertainty in the experimental determination.

We must stress that the fitting procedure can be quite arbitrary, especially when there are peaks with very close wavenumber and that the assessment of the quality of our predictions should be done preferably considering integrals in wide spectral areas, resulting by the convolution of more than one Raman component. On the other hand, in the absence of a physically reasonable criterion, which could constrain the choice of the Full Width at Half Maximum (FWHM) parameters, the Raman cross section attributed to some individual components, which are described—by the deconvolution procedure—as very broad Lorentzian bands, could be largely overestimated. For this reason, we explored alternative procedures for the spectra deconvolution, introducing a few fixed FWHM values, for some bands (see Table S5). The choice of the fixed FWHM values, illustrated in SI, was performed aiming simply to test whether this strategy could improve the agreement between theory and experiment. The results reported in Table S5 show that we can obtain a better description, without affecting substantially the quality of the fit. For instance, the Err% = 41 of the 5E(LO) band can be reduced to 16.7%, if a value of 15 cm^{-1} is adopted for its FWHM, instead of the value of 20.5, obtained without constraints on band widths.

The spectrum corresponding to the two equivalent $Z(XX)\overline{Z}/Z(YY)\overline{Z}$, at variance with respect to the $Y(XX)\overline{Y}$ configuration (Table 4 and Figure 3), shows many Raman intensities of comparable strength. Also, in this case, the 4A_1 mode is the dominant bands, about 10 times stronger than the others.

Also, in this case, a spectrum deconvolution is required, because several modes, especially in the region below 450 cm^{-1}, show very close wavenumbers. In particular, there are four pair of bands showing so large overlap that it is convenient to sum their individual intensities when comparing with the theoretical predictions. So the large difference (about 50%) in intensity for 6E dramatically reduces when considering the joint contribution with 5E.

As for the $Y(XX)\overline{Y}$ spectrum, in Table S6, we illustrate that it is possible to improve the agreement between the individual experimental and computed band intensities of the $Z(XX)\overline{Z}$ spectrum, while adopting a different strategy for bands deconvolution, namely, by introducing fixed FWHM values for some selected peaks.

A further step in the analysis of the Raman response of LO phonons can be done by considering the contribution to Raman polarizability coming from the term involving the second order susceptibility ($\chi^{(2)}$ correction).

TABLE 5 α_{xx} computed values for the LO modes of $LiNbO_3$ and their $\chi^{(2)}$ correction

	mode #	wavenumber (cm^{-1})	α_{xx} ($Å^2$ $amu^{-1/2}$)	$\chi^{(2)}$ correction ($Å^2$ $amu^{-1/2}$)	% variation α_{xx}	Raman Activity ($Å^4$ amu)	Raman Activity (no correction) ($Å^4$ amu)
E modes	1	195	0.588	−0.024	−4	0.35	0.38
	2	242	1.209	−0.007	−1	1.46	1.48
	3	296	1.983	−0.023	−1	3.93	4.02
	4	344	0.422	−0.016	−4	0.18	0.19
	5	368	1.555	−0.007	0	2.42	2.44
	6	431	3.394	0.065	2	11.52	11.09
	7	**466**	**0.001**	**−0.088**	**−99**	0.00	0.01
	8	663	1.121	0.027	2	1.26	1.20
	9	**892**	**3.217**	**−0.477**	**−13**	**10.35**	**13.65**
A_1 modes	1	276	2.651	0.093	4	7.03	6.54
	2	343	3.696	0.014	0	13.66	13.56
	3	**434**	**6.012**	**2.044**	**52**	**36.15**	**15.75**
	4	**883**	**14.293**	**−6.589**	**−32**	**204.30**	**436.08**

Note: In column V, the percentage variation of α_{xx} after $\chi^{(2)}$ correction is reported. The last two column report computed Raman activity of the LO modes of E and A_1 species in the polarized $Y(XX)\overline{Y}$ and $Z(XX)\overline{Z}$/ $Z(YY)\overline{Z}$ spectra, respectively. Boldface characters highlight modes largely affected by the $\chi^{(2)}$ correction.

In Table 5, we report the percentage changes of the Raman polarizability component $\alpha^k_{xx} = \frac{\partial \alpha_{xx}}{\partial Q_k}$, which rules the Raman intensity of the LO Q_k modes (E species) in the spectrum of Figure 2/Table 3 and the LO Q_k modes (A_1 species) in the spectrum of Figure 3/Table 4. For LO E modes, the $\chi^{(2)}$ correction is almost negligible, except for 7E and, to a lesser extent, for 9E. However, the 100% change of 7E results from the practically null Raman activity of this mode; the variation of the polarizability value after the $\chi^{(2)}$ correction is very small. Very large $\chi^{(2)}$ corrections concern $3A_1$ and $4A_1$ modes, namely, the first and the second LO modes, according to their Raman intensity. The $\chi^{(2)}$ correction doubles the Raman activity for $3A_1$ and reduces by a factor 2 the one of $4A_1$. This behaviour is very close to the one reported in Hermet et al.[20] Moreover, the $\chi^{(2)}$ correction proves to be of fundamental importance for a correct prediction of our observed intensity pattern (Table 4). For instance, the observed intensity ratio between $3A_1$ (LO) and $4A_1$ (LO) is 0.35, in nearly perfect agreement with the theoretical prediction based on $\chi^{(2)}$ corrected Raman intensities, while the use of non-corrected intensities would give a predicted ratio of 0.08, only about 20% of the experimental one.

A_1 (LO) band intensity has been used as reference (intensity value arbitrarily set to 1), to obtain the relative intensity values reported in Table 4. Because of the doubling of A_1 (LO) band intensity before $\chi^{(2)}$ correction, the normalization factor doubles, and the non-corrected relative intensities decrease by about 50%. This is a consequence of the fact that most of the bands are not affected (TO modes) or scarcely affected (LO modes different from $3A_1$ and $4A_1$) by the $\chi^{(2)}$ correction.

We note that, if the theoretical data reported in Table 4 were replaced with halved values, the agreement with the experimental intensity pattern would be remarkably worse.

According to Hermet et al.,[20] the $\chi^{(2)}$ correction also affects the intensity of the LO 9E mode in the Raman spectrum corresponding to $X(ZX)Y$ configuration, which depends on the α_{zx} component. Our experimental data concern $Y(XX)\overline{Y}$ setup, where intensities are ruled by the α_{xx} component; Table 5 shows that a non-negligible $\chi^{(2)}$ correction also affects this component of the 9E mode, giving rise to a decrease of the 30% of its Raman intensity in the spectrum of Figure 3.

4 | CONCLUSIONS

We have presented a detailed analysis of the experimental polarized Raman spectra of a single crystal of $LiNbO_3$ in its room temperature *R3c* phase. Raman experiments have been carried out in backscattering geometry, selecting the three different crystal orientation/polarization setups, which provide the $Y(XX)\overline{Y}$ spectrum and the two equivalent $Z(XX)\overline{Z}/Z(YY)\overline{Z}$ spectra. In both $Y(XX)\overline{Y}$

and $Z(XX)\overline{Z}/Z(YY)\overline{Z}$ configurations, we can observe Raman transitions associated to TO and LO modes belonging to the Raman active A_1 and E irreducible representations of the C_{3v} symmetry point group. The $Y(XX)\overline{Y}$ spectrum shows E LO modes + A_1 TO modes, while $Z(XX)\overline{Z}/Z(YY)\overline{Z}$ spectra show E TO modes + A_1 LO modes, thus providing a set of 26 independent observables (peaks wavenumbers) and the corresponding relative Raman cross sections.

The collection of these experimental data allows a thorough analysis of the performance of Quantum Mechanical simulations we carried out by means of DFT periodic boundary conditions LCAO calculations, as implemented in the CRYSTAL software.

The analysis here presented complements a study recently published by some of the present authors,[16] which was limited to the prediction of the Raman transitions associated to TO phonons of $LiNbO_3$. In particular, the careful comparison between experimental and theoretically predicted observables (viz., LO phonons Raman wavenumbers and bands intensities) allowed to assess the performance of the theoretical approach, highlighting several relevant features:

i. The level of theory adopted is suitable for an excellent prediction of the polarized Raman spectra, both in wavenumbers—the MAE on the full set of 26 modes is as small as 6.4 cm^{-1}—and intensities.
ii. The accuracy of the prediction for LO phonons (vibrational wavenumbers and Raman activities) is comparable to that obtained for TO modes.

iii. TO/LO splits are reproduced well and can be rationalized with the help of the overlap matrix between the corresponding eigenvectors and considering the correction to the dynamical matrix, coming from the large Born Charges associated to some modes.

The Raman tensors of LO modes have been calculated both by including and by neglecting the $\chi^{(2)}$ correction. The comparison of these results demonstrates that the correction of LO modes activity is mandatory to reproduce the experimental intensity pattern in both $Y(XX)\overline{Y}$ and $Z(XX)\overline{Z}/Z(YY)\overline{Z}$ spectra.

iv. According to Hermet et al.,[20] our simulation of the Raman spectrum indicates that the LO mode 4E corresponds to a very weak feature observed at 332 cm^{-1}. The transition has been identified following the indication from theory, thus suggesting that the assignment proposed in Fontana and Bourson[36] should be revised by removing the weak/broad feature observed at 186 cm^{-1} from the list of the fundamental vibrational transitions of $LiNbO_3$.

ACKNOWLEDGEMENTS

The CQC-IMS is financially supported by the Portuguese Science Foundation ("Fundação para a Ciência e a Tecnologia" - FCT) – Projects CQC UIDB/00313/2020 and UIDP/00313/2020 (National Funds). Access to instruments from Laser-Lab Coimbra is gratefully acknowledged. B.A.N. acknowledges FCT for the SFRH/BD/129852/2017 PhD Scholarship. Open Access Funding provided by Politecnico di Milano within the CRUI-CARE Agreement.

DATA AVAILABILITY STATEMENT

Data available on request from the authors; Data available in article supplementary material

ORCID

Bernardo A. Nogueira https://orcid.org/0000-0002-1756-377X
Michel Rérat https://orcid.org/0000-0002-8459-5499
Rui Fausto https://orcid.org/0000-0002-8264-6854
Chiara Castiglioni https://orcid.org/0000-0002-6945-9157
Roberto Dovesi https://orcid.org/0000-0002-9821-9128

REFERENCES

[1] B. Schrader, D. Bougeard, *Infrared and Raman spectroscopy: Methods and applications*, VCH, Weinheim **1995**.
[2] B. H. Stuart, *Infrared spectroscopy: Fundamentals and applications*, Wiley, Chichester **2004**.
[3] P. J. Larkin, *Infrared and Raman spectroscopy: Principles and spectral interpretation*, Elsevier, Amsterdam **2011**.
[4] A. A. Bunaciu, H. Y. Aboul-Enein, V. D. Hoang, *TrAC, Trends Anal. Chem.* **2015**, *69*, 14.
[5] G. Keresztury, Raman spectroscopy, in *Theory in handbook of vibrational spectroscopy*, (Ed: J. M. Chalmers), John Wiley & Sons, Ltd, Chichester **2006**.
[6] C. Castiglioni, Theory of vibrational spectroscopy of polymers, in *Vibrational spectroscopy of polymers*, (Eds: N. J. Everall, J. M. Chalmers, P. R. Griffiths) Vol. 15, Wiley, Chichester, UK **2007** 455.
[7] D. A. Long, *Raman spectroscopy*, McGraw-Hill, New York **1977**.
[8] T. C. Damen, S. P. S. Porto, B. Tell, *Phys. Rev.* **1966**, *142*, 570.
[9] T. R. Gilson, P. J. Hendra, *Laser Raman spectroscopy*, Wiley, London **1970**.
[10] G. Turrell, *Infrared and Raman spectra of crystals*, Academic Press, London **1972**.
[11] G. R. Wilkinson, Raman spectra of ionic, covalent, and metallic crystals, in *The Raman effect: Applications*, (Ed: A. Anderson) Vol. 2, Marcel Dekker, New York **1973** 811.
[12] M. de la Pierre, R. Demichelis, R. Dovesi, Vibrational spectroscopy of minerals through ab initio methods, in *Molecular*

modeling of geochemical reactions: An introduction, (Ed: J. B. Kubicki) Vol. 341, John Wiley & Sons, Ltd, Chichester **2007**.
[13] L. Maschio, B. Kirtman, M. Rérat, R. Orlando, R. Dovesi, *J. Chem. Phys.* **2016**, *139*, 164101.
[14] M. de la Pierre, C. Carteret, R. Orlando, R. Dovesi, *J. Comput. Chem.* **2013**, *34*, 1476.
[15] F. Pascale, S. Salustro, A. M. Ferrari, M. Rérat, P. D'Arco, R. Dovesi, *Theor. Chem. Acc.* **2018**, *137*, 1.
[16] B. A. Nogueira, A. Milani, C. Castiglioni, R. Fausto, *J. Raman Spectrosc.* **2021**, *52*, 995.
[17] R. Dovesi, V. R. Saunders, C. Roetti, R. Orlando, C. M. Zicovich-Wilson, F. Pascale, B. Civalleri, K. Doll, N. M. Harrison, I. J. Bush, P. D'Arco, M. Llunell, M. Causà, Y. Noël, L. Maschio, A. Erba, M. Rerat, S. Casassa, CRYSTAL17 User's Manual. University of Torino, **2017**, Torino, Italy.
[18] V. Caciuc, A. Postnikov, G. Borstel, *Phys. Rev. B - Condens. Matter Mater. Phys.* **2000**, *61*, 8806.
[19] K. Parlinski, Z. Li, *Phys. Rev. B - Condens. Matter Mater. Phys.* **2000**, *61*, 272.
[20] P. Hermet, M. Veithen, P. Ghosez, *J. Phys. Condens. Matter* **2007**, *19*, 456202.
[21] R. Dovesi, A. Erba, R. Orlando, C. M. Zicovich-Wilson, B. Civalleri, L. Maschio, M. Rérat, S. Casassa, J. Baima, S. Salustro, B. Kirtman, *Wiley Interdiscip. Rev. Comput. Mol. Sci.* **2018**, *8*, e1360.
[22] C. Lee, W. Yang, R. G. Parr, *Phys. Rev. B* **1988**, *37*, 785.
[23] J. Laun, D. V. Oliveira, T. Bredow, *J. Comput. Chem.* **2018**, *39*, 1285.
[24] D. V. Oliveira, J. Laun, M. F. Peintinger, T. Bredow, *J. Comput. Chem.* **2019**, *40*, 2364.
[25] M. F. Peintinger, D. V. Oliveira, T. Bredow, *J. Comput. Chem.* **2013**, *34*, 451.
[26] M. Ferrero, M. Rérat, R. Orlando, R. Dovesi, *J. Comput. Chem.* **2008**, *29*, 1450.
[27] M. Ferrero, M. Rérat, R. Orlando, R. Dovesi, I. J. Bush, *J. Phys. Conf. Series* **2008**, *117*, 12016.
[28] L. Maschio, B. Kirtman, M. Rérat, R. Orlando, R. Dovesi, *J. Chem. Phys.* **2013**, *139*, 164101. PMID: and 164102.
[29] S. C. Abrahams, J. M. Reddy, J. L. Bernstein, *J. Phys. Chem. Solids* **1966**, *27*, 997.
[30] S. Baroni, S. de Gironcoli, A. Dal Corso, P. Giannozzi, *Rev. Mod. Phys.* **2001**, *73*, 515.
[31] W. D. Johnson Jr., *Phys. Rev. B* **1970**, *1*, 3494.
[32] Y. Repelin, E. Husson, F. Bennani, C. Proust, *J. Phys. Chem. Solids* **1999**, *60*, 819.
[33] H. Kuzmany, *Solid-state spectroscopy*, Springer, Berlin **1998**.
[34] R. F. Schaufele, M. J. Weber, *Phys. Rev.* **1966**, *152*, 705.
[35] R. Loudon, *Adv. Phys.* **1964**, *13*, 423.
[36] M. D. Fontana, P. Bourson, *Appl. Phys. Rev.* **2015**, *2*, 040602.
[37] A. S. Barker, R. Loudon, *Phys. Rev.* **1967**, *158*, 433.
[38] R. Claus, G. Borstel, E. Wiesendanger, L. Steffan, *Phys. Rev. B* **1972**, *6*, 4878.
[39] V. S. Gorelik, P. P. Sverbil, *Inorg. Mater.* **2015**, *51*, 1104.
[40] I. P. Kaminow, W. D. Johnston, *Phys. Rev.* **1967**, *160*, 519.
[41] A. Ridah, P. Bourson, M. D. Fontana, G. Malovichko, *J. Phys. Condens. Matter* **1997**, *9*, 9687.
[42] X. Yang, G. Lan, B. Li, H. Wang, *Phys. Status Solidi* **1987**, *142*, 287.
[43] A. Erba, J. Maul, M. Ferrabone, P. Carbonnière, M. Rérat, R. Dovesi, *JCTC* **2019**, *15*, 3755.
[44] A. Erba, J. Maul, M. Ferrabone, R. Dovesi, M. Rérat, P. Carbonnière, *JCTC* **2019**, *15*, 3766.
[45] P. Carbonnière, A. Erba, F. Richter, R. Dovesi, M. Rérat, *JCTC* **2020**, *16*, 3343.
[46] Thermo Fisher Scientific Inc. Omnic software (version 8.2.0.387).

SUPPORTING INFORMATION

Additional supporting information can be found online in the Supporting Information section at the end of this article.

How to cite this article: B. A. Nogueira, M. Rérat, R. Fausto, C. Castiglioni, R. Dovesi, *J Raman Spectrosc* **2022**, 1. https://doi.org/10.1002/jrs.6426